

**Article**

**$\gamma$ -Aluminum Oxide Nanopowder ( $\gamma$ -Al<sub>2</sub>O<sub>3</sub> NPs), Methyl Red Dye, And Dill Plant Dye As a Luminous Solar Cell Concentrator(LSC)**

**Muslim Jassim Mohammed Al-Sa'abri<sup>1</sup>, Aqeel Mahdi Jreo Alduhaidahawi<sup>2</sup>,**

1Emil: maslimj.alsabari@student.uokufa.edu.iq.

2Emil: aqeelm.alduhaidahawi@uokufa.edu.iq

**1,2 Department of Chemistry, College of Science, Kufa University, Najaf  
54001, Iraq.**

**Abstract**

Aluminum oxide nanoparticle were prepared by electrochemical method as it is an easy and cheap method and gives high purity results, and the prepared materials were characterization by using techniques XRD, SEM, TEM, EDX, AFM and UV-VIS this technique showed high purity of  $\gamma$ -AL<sub>2</sub>O<sub>3</sub>NPs and in this investigation, a luminescent concentrator composed of  $\gamma$ -aluminum oxide ( $\gamma$ -Al<sub>2</sub>O<sub>3</sub> NPs), known for its robust catalytic capabilities, methyl red dye, and Dill (*Anethum graveolens*) dye was employed. The outcomes of amalgamating these concentrates, either collectively or singly, with the silicon solar cell, demonstrated a remarkable augmentation in the cell's efficiency. The increment ranged from 16% to 79.7% for the Dill (*Anethum graveolens*) dye and nano  $\gamma$ -aluminum oxide combined with methyl red dye, respectively. This surge signifies a stride towards the optimal trajectory in the realm of advancing scientific inquiry to attain the utmost efficiency feasible through the use of luminescent solar concentrators (LSCs).

**Keyword:**  $\gamma$ -Aluminum oxide,  $\gamma$ -Al<sub>2</sub>O<sub>3</sub> NPs, Electrochemical method, Silicon cell, luminescent solar concentrators (LSC).

**1.Introduction**

Nanoscience is one of the most widely used fields of science in the last three decades because it has many and wide applications in many fields. For example, but not limited to, nanoscience has entered the fields of industry, agriculture,

medicine, national security, and energy (1). Nanomaterials are materials with structures sized between (1-100 nm) on the nanoscale. They are distinguished by their large surface area, flexibility hardness, tensile, strength, and enhanced optical and magnetic properties, surpassing those of bulk materials. (2), (3). With the world looking for more sustainable energy technologies in order to combat climate change, photovoltaic (PV) technologies have shown a huge potential to take the lead in this challenge (4), Solar energy usage is expanding quickly due to the negative effects of conventional fossil fuel-based energy sources on the environment Solar energy is a reliable and abundant resource, and solar cells are an efficient and useful way to capture it. The sun delivers  $1367 \text{ W/m}^2$  of solar energy into the atmosphere, nearly  $1.8 \times 10^{11}$  (MW) of solar energy is absorbed globally, sufficient to cover the world's power requirement (5). Speaking of solar cells, nano  $\gamma$ -Aluminum oxide stands out as light weight, high strength, resistance to corrosion, and excellent electrical and thermal conductivities. These qualities have made it a popular choice for uses in catalysts and optoelectronic devices.  $\text{Al}_2\text{O}_3$  exists in several metastable polymorphs, including  $\gamma$ ,  $\eta$ ,  $\delta$ ,  $\theta$ , and  $\chi$  phases, as well as the stable  $\alpha$ - $\text{Al}_2\text{O}_3$ , also known as corundum. The amorphous, gamma, and alpha forms of  $\text{Al}_2\text{O}_3$  are of particular interest technologically and can be created using solid-phase, liquid-phase, and gas-phase processes. The gamma form is sought after for its large surface area and is used in catalysis, while the alpha form's polycrystalline nature makes it ideal for glass and ceramic applications (6), (7). To enhance the efficiency of solar cells and reduce waste of solar energy, the luminous solar concentrator (LSC) has emerged and was found as one of the best ways to enhance the productivity of conversion efficiency using the method of concentrating sunlight (8) (9).

## **2. Experimental details**

High-purity materials were used to prepare nano- $\gamma$ -aluminum oxide ( $\gamma$ - $\text{Al}_2\text{O}_3$  NPs) by the electrochemical method, as it is considered a cheap and easy method with a high-purity product.

### **2.1 Materials**

A high purity materials were used in order to achieve real feasibility of this research, as follows Potassium chloride (98% CDH India), Polyvinylpyrrolidone (PVP K30) (99% CDH India), Titanium foil 98% Laboratory Chemical India, Ethanol absolute 99% Sigma. USA, Methyl Red 98% Thomas baker, Dill (*Anethum graveolens*), Silicon cell [Polycrystalline Chinese company (PMK1711) Size (39 \*22 mm), Max power 0.14 Mw, rated voltage 0.5 V, Rated

current 0.28 A, Quantity 50 pcs/lot)] light source.

## **2.2 Electrochemical synthesis of $\gamma$ -Al<sub>2</sub>O<sub>3</sub> NPs**

$\gamma$ -aluminum oxide nanoparticles ( $\gamma$ -Al<sub>2</sub>O<sub>3</sub> NPs) are synthesized by submerging aluminum electrodes in an electrolyte solution with a stabilizer (pvp), under specific voltage. The mixture is stirred magnetically, then the nanoparticles are collected, washed, dried, and calcined. The electrolysis cell, made of plastic (10 cm x 4 cm x 10 cm, 400 ml v) is cleaned with ethanol and deionized water. It's filled with 5 ml KCl (10% wt./v) and (10 ml) PVP K30 (10% wt./v), topped up to 200 ml with deionized water. Two aluminum electrodes (0.25 mm thick, 1 cm x 8 cm for cathode, 2 cm x 8 cm for anode) are immersed and connected to a power supply (0-30 volts, 0-5A), with a magnetic bar stirring the solution [(10, 11)].as shown in figure 1.1



**Figure 1.1 Electrochemical cell system**

## **3. Result and Discussion**

X-ray diffraction (XRD), Transmission Electron Microscopy (TEM), Field Emission Scanning Electron Microscopy (FESEM), Energy Dispersive X-ray Spectroscopy (EDX), Atomic Force Microscopy (AFM), and Ultraviolet-Visible Spectroscopy (UV-Vis) techniques were utilized to characterize nanostructured  $\gamma$ -aluminum oxide around the sample. The results of tests of the above devices showed the formation of gamma-type aluminum oxide nanostructures. The table 1.1 shows the technologies used, the companies that manufacture them, and their location.

**Table 1.1 All information about the technologies used**

No.	Device	Name and origin	location
1.	Field Emission Scanning Electron Microscopy (FESEM)	TESCAN BRNO Mira3LMU	Ferdowsi faculty /Mashhad University /Iran
2.	X-Ray Diffraction (XRD)	/6000Shimadzu, Japan	Engendering faculty / Kufa university
3.	Atomic Force Microscopy(AFM)	CSPM-4000/Hitachi, Japan	Ferdowsi faculty /Mashhad University /Iran
4.	Transmission Electron Microscopy (TEM)	CM300 Philips germen	Ferdowsi faculty /Mashhad University /Iran
5.	Energy Disperse X-Ray Spectroscopy (EDX)	MIRA3 Shimadzu japan	Ferdowsi faculty /Mashhad University /Iran
6.	UV-Vis Spectrophotometer Double Beam	Shimadzu UV 1650 PC Japan	Physics faculty / Kufa university
7.	Solar module analyzer	PROVA 200A China INC company	Physical department / Science faculty/ Kufa university

### 3.1 X-Ray Diffraction Analysis for $\gamma$ -Al<sub>2</sub>O<sub>3</sub> NPs

By Using a diffraction setup with Cu-K1 of ( $\lambda=1.54060$  A) under 40 kv and 30 mA in the range of 2 thetas ( $2\theta$ ) from 10 to 80,  $\gamma$ -Al<sub>2</sub>O<sub>3</sub> NPs were studied. Several diffraction peaks at  $2\theta$  values of ( $32.61^\circ, 35.84^\circ, 38.789^\circ, 44.843^\circ, 53.663^\circ, 58.81^\circ, 65.635^\circ$ ) which are compatible to Miller indices (220), (311), (222), (400), (511) and (440) that characterize the  $\gamma$ -Al<sub>2</sub>O<sub>3</sub> NPs. The size of  $\gamma$ -Al<sub>2</sub>O<sub>3</sub> NPs calculated by using Scherrer equation JCPDS Card No.29-0063 (12) The X-ray Diffraction Analysis also showed, in addition to 2-theta, the FWHM (Full Width at Half Maximum. It's a term used to describe the width of a peak in a spectrum at the point where its intensity is half of the maximum intensity (13) and crystal size, as the average size was approximately (8 nm) as shown in table 1.2 and figure 1.2 (14).

**Table 1.2 X-Ray Diffraction data of  $\gamma$ -Al<sub>2</sub>O<sub>3</sub> NPs.**

2-Theta	FWHM	Crystal size (nm)
10.686	0.797	11
13.404	1.124	7
18.063	1.008	8
19.626	1.033	8
23.287	0.743	12
24.975	1.057	8

26.624	1.279	7
28.193	1.279	7
31.011	1.258	7
32.61	1.206	7
35.84	1.288	7
38.789	1.424	6
44.843	1.452	6
53.663	0.631	15
58.81	1.793	5
65.635	1.333	7

Average size : 8 nm

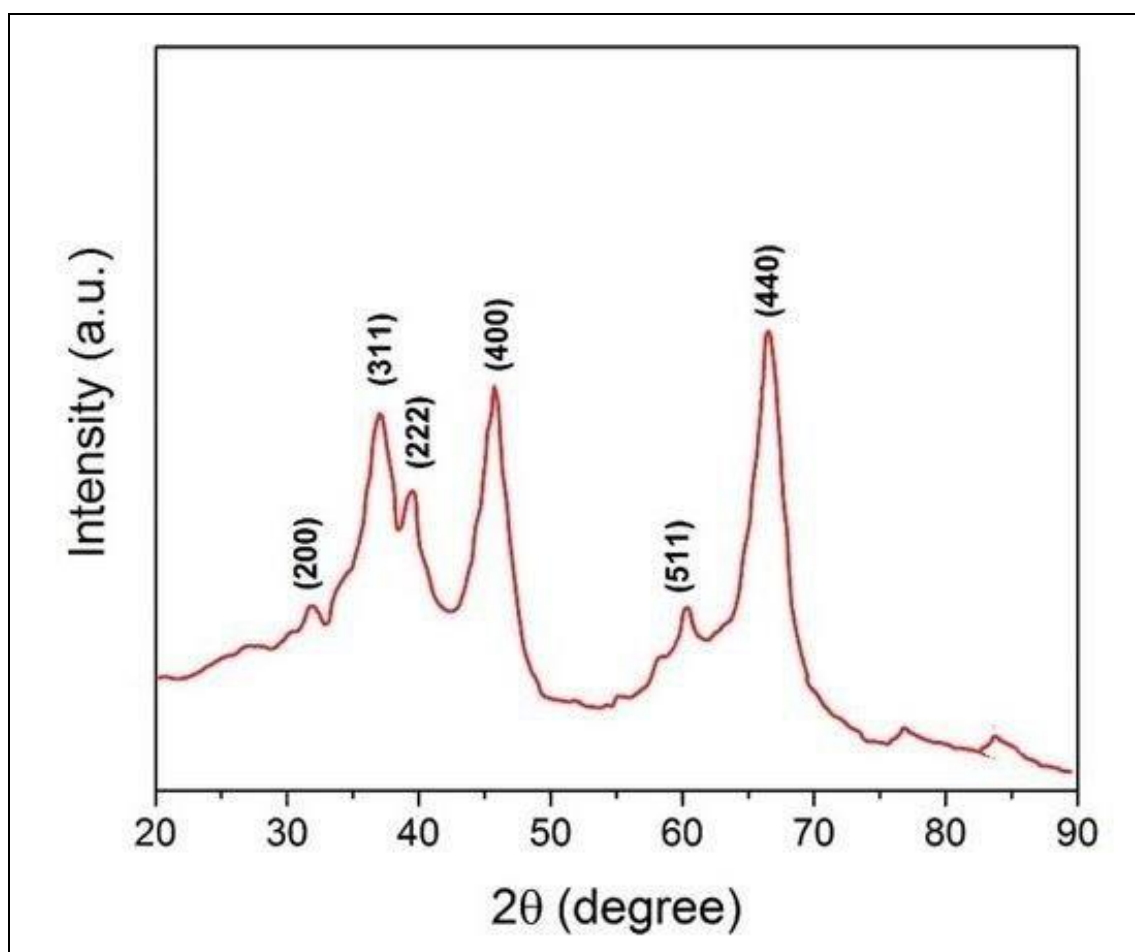
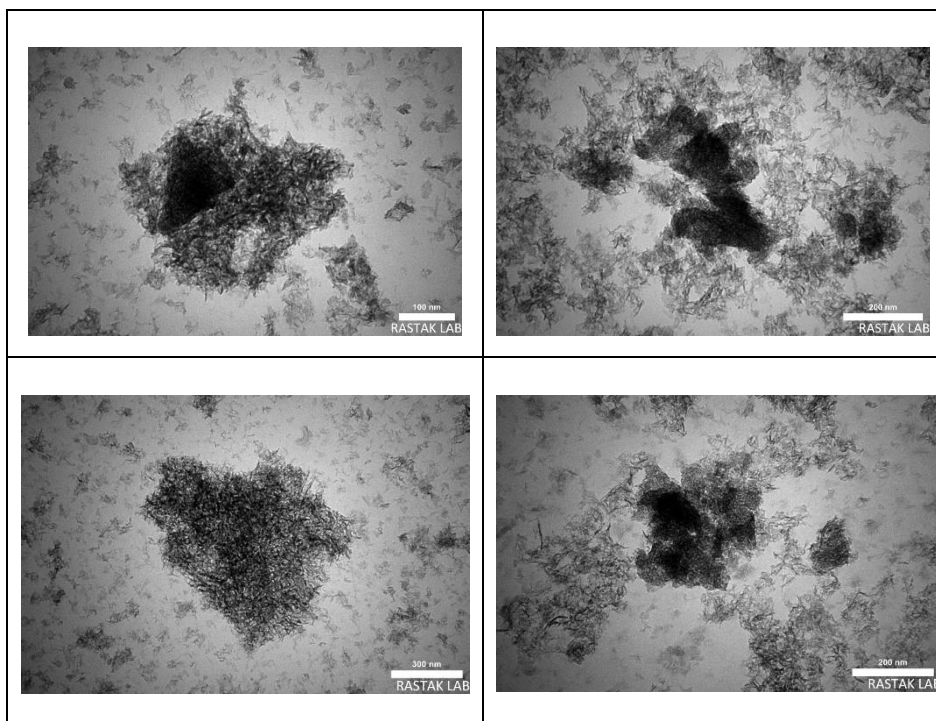


Figure 1.2 X-Ray Diffraction pattern of  $\gamma\text{-Al}_2\text{O}_3$  NPs

### 3.2 Transmission Electron Microscopy (TEM) Analysis for $\gamma\text{-Al}_2\text{O}_3$ NPs

The transmission electron microscope shows the morphological properties of the nano powder surface, as is evident in the images whose magnifications vary

from 100 nm to 200 nm, the nanowire of the  $\gamma$ -aluminum oxide  $\gamma$ -Al<sub>2</sub>O<sub>3</sub> NPs (15). as shown in Figure 1.3.



**Figure 1.3 TEM images of  $\gamma$ -Al<sub>2</sub>O<sub>3</sub> NPs.**

Using Origin software for TEM picture analysis, the size of the  $\gamma$ -aluminum oxide ( $\gamma$ -Al<sub>2</sub>O<sub>3</sub> NPs) nanocrystal was measured, reaching (27.205 nm) this nano size gives high catalytic efficiency because it is within the nanoscale (1-100 nm), as shown in Figure 1.4.

	N total	Mean	Standard Deviation	Sum	Minimum	Median	Maximum
D	50	27.20558	11.80228	1360.279	13.329	25.868	79.70

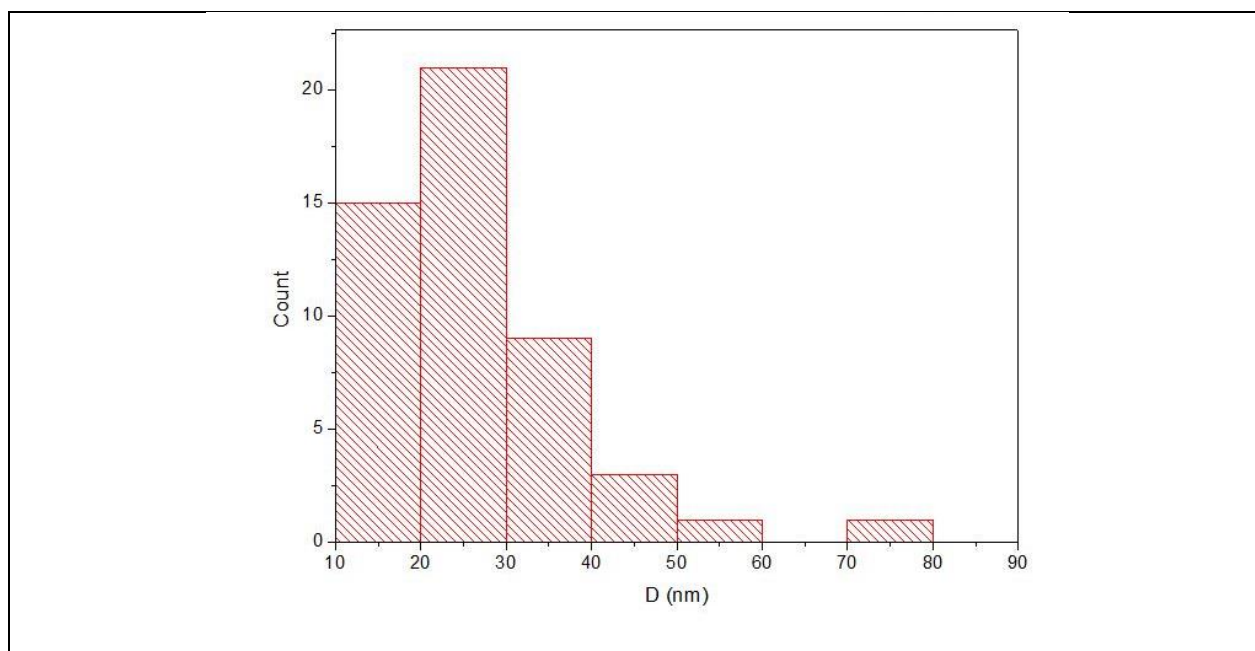
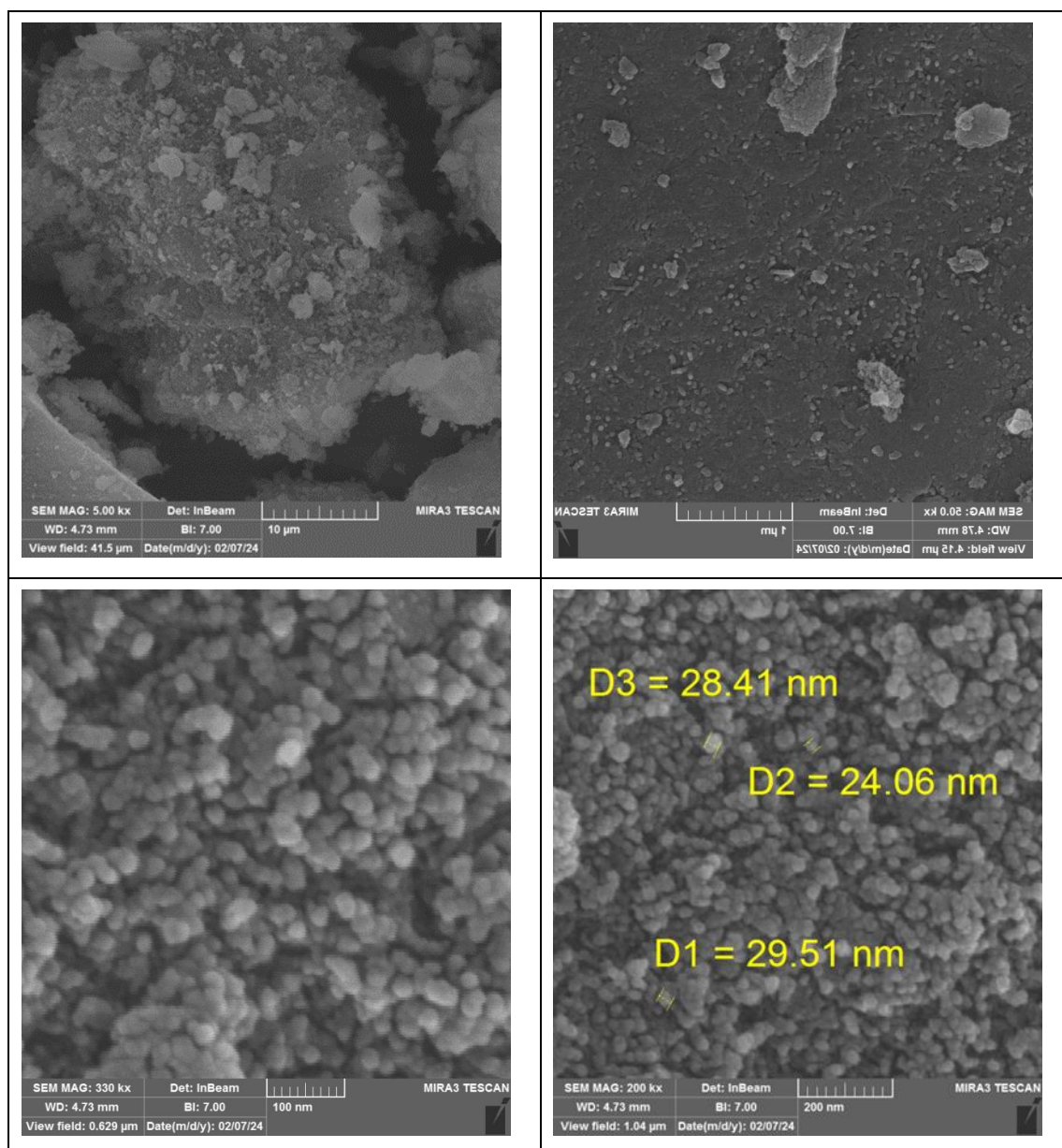


Figure 1.4 show size of  $\gamma\text{-Al}_2\text{O}_3$  NPs by origin software

### 3.3 The Field Emission Scanning Electron Microscope (FESEM) Analysis for $\gamma\text{-Al}_2\text{O}_3$ NPs

A scanning electron microscope (FESEM) was used for a sample of nano-powdered  $\gamma$ -aluminum oxide ( $\gamma\text{-Al}_2\text{O}_3$ ). The surface topography of powder is clearly shown in Figure 1.5, where the images showed the nano-oxide particles and their formation resembling bunches of nanowire nanoparticles(16) These images are considered further evidence of the correct composition of the  $\gamma\text{-Al}_2\text{O}_3$  NPs sample type, as shown below



**Figure 1.5** FESEM images of  $\gamma$ -Al<sub>2</sub>O<sub>3</sub> NPs.

### 3.4 Energy Dispersive X-Ray Spectroscopy (EDX) for $\gamma$ -Al<sub>2</sub>O<sub>3</sub> NPs

The results of the energy dispersive X-ray (EDX) examination in Figure 1.6 showed clear peaks for oxygen and aluminum. This technique demonstrated the high purity of aluminum oxide nanoparticles  $\gamma$ -Al<sub>2</sub>O<sub>3</sub>, as well as the percentages attached to the diagram, which proved that the percentage of oxygen was greater than that of aluminum, as the percentage was 66% and 33%, respectively. (17).

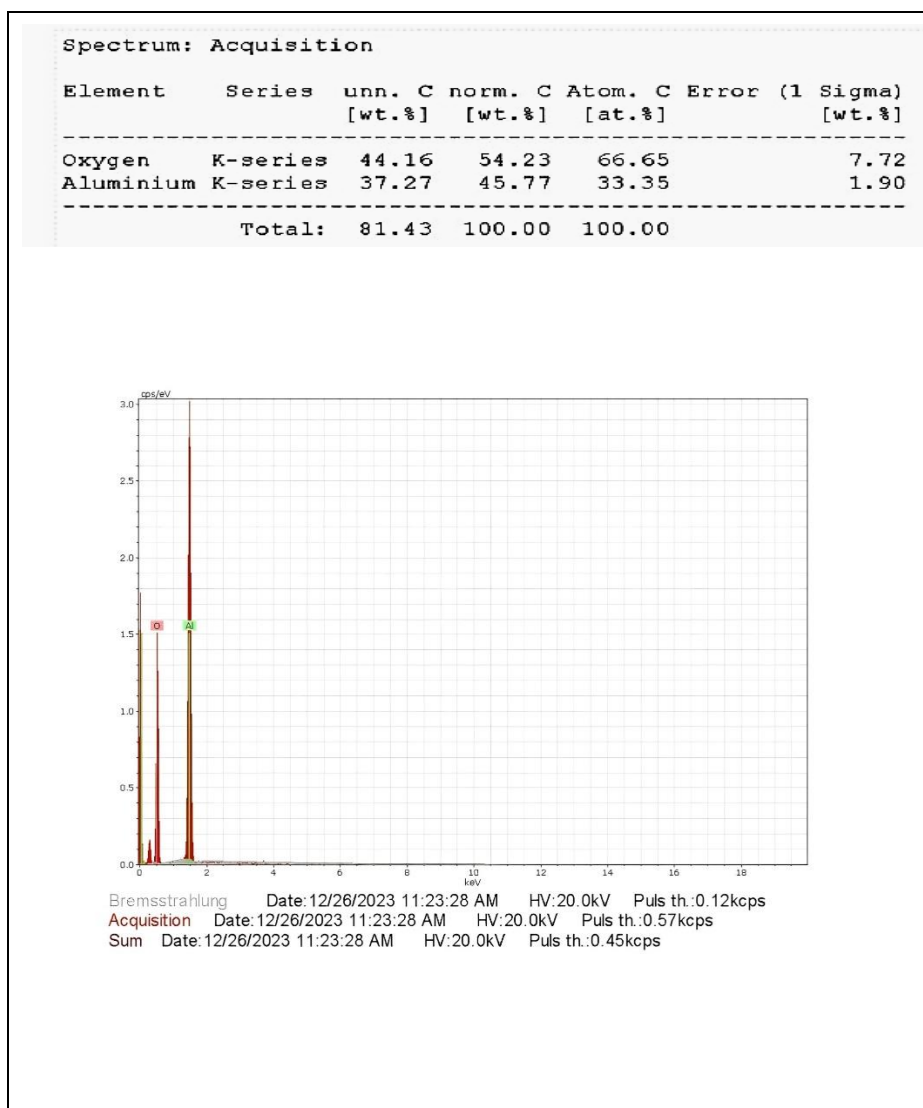


**Figure 1.6 (EDX - Ray of  $\gamma$ -Al<sub>2</sub>O<sub>3</sub> NPs**

### 3.5 Atomic Force Microscopy (AFM) Analysis for $\gamma$ -Al<sub>2</sub>O<sub>3</sub> NPs

Using an Atomic Force Microscope (AFM) on a  $\gamma$ -aluminum oxide ( $\gamma$ -Al<sub>2</sub>O<sub>3</sub>) nanoparticle specimen have disclosed a comprehensive view of the surface morphology. In the AFM depictions, color shifts correspond to variations in structural height, with darker tones suggesting lower regions and lighter tones denoting elevated areas. Significant AFM metrics encompass Surface Skewness, which is the asymmetry of the surface contours, Roughness Average (Ra), indicating the mean deviation from the central plane, and Root Mean Square (Rq), which is the square root of the mean of the squared deviations. The AFM study yields information regarding the distribution of nanoparticle sizes, their

mean diameter, and the consistency of the surface, as illustrated in Figure 1.7 via uniform 2D and 3D representations (18).

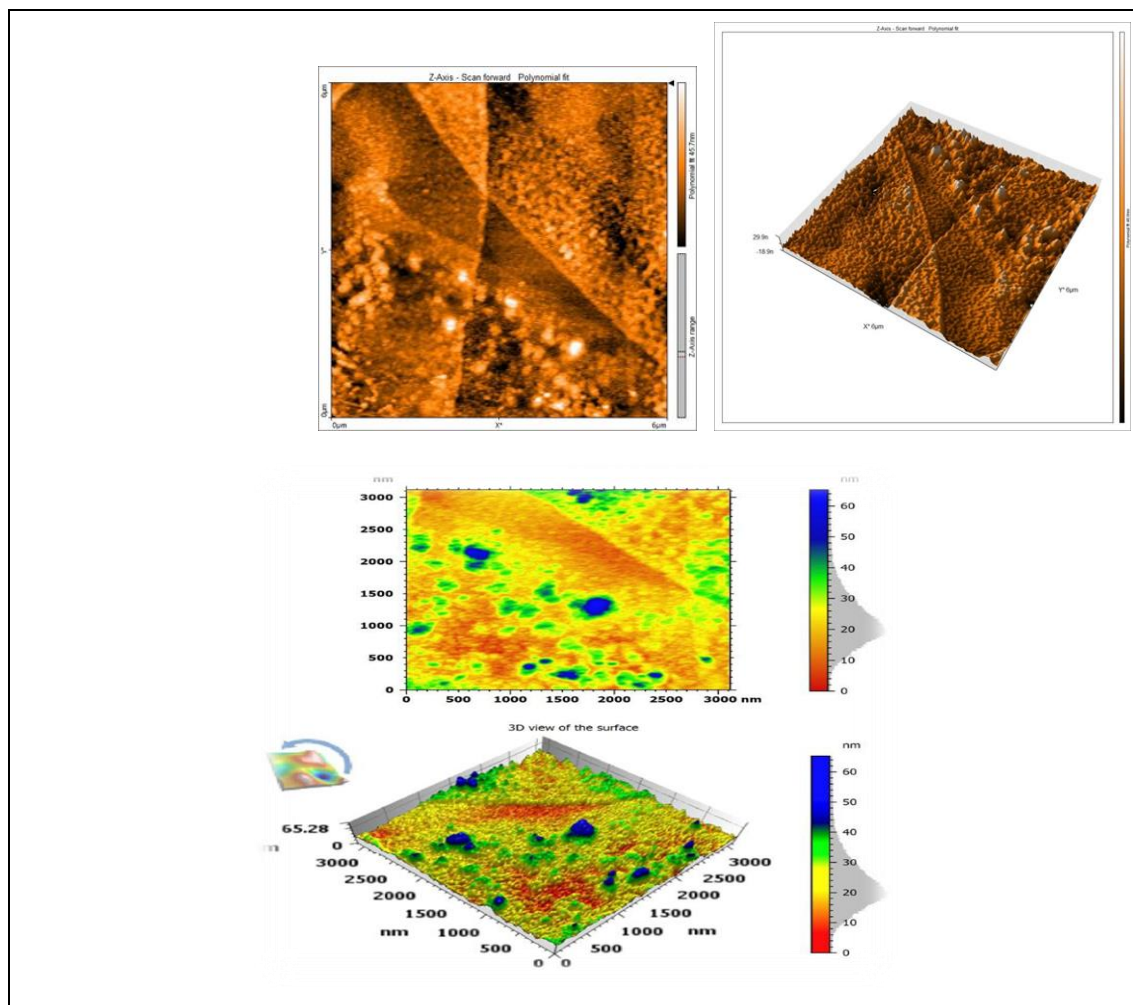


Figure 1.7 through 2D and 3D homogenous images

### 3.6 Ultra Violet -Visible spectroscopy (UV-Vis) for $\gamma$ -Al<sub>2</sub>O<sub>3</sub> NPs

The energy band gap of  $\gamma$ -aluminum oxide nanoparticles ( $\gamma$ -Al<sub>2</sub>O<sub>3</sub> NPs) synthesized electrochemically was ascertained by analyzing the UV-Visible spectral data, focusing on the wavelengths with significant absorption. To calculate the energy gap (Eg) values, Tauc's method was employed, a plot of  $(\alpha h\nu)^2$  against  $(h\nu)$  curves. The extrapolation of the linear portion of plot at  $(\alpha h\nu)^2 = 0$  gives the match Eg (eV) value, Figure 1.8, the plot of  $(\alpha h\nu)^2$  against  $(h\nu)$  curves of electrochemically prepared  $\gamma$ -Al<sub>2</sub>O<sub>3</sub> NPs (19).

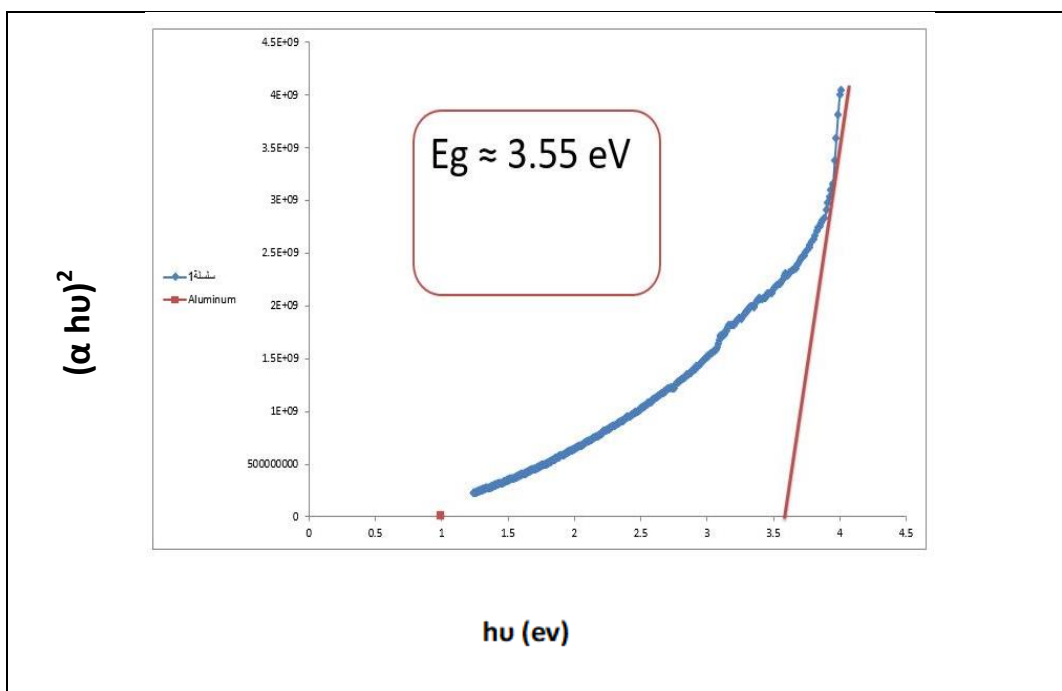
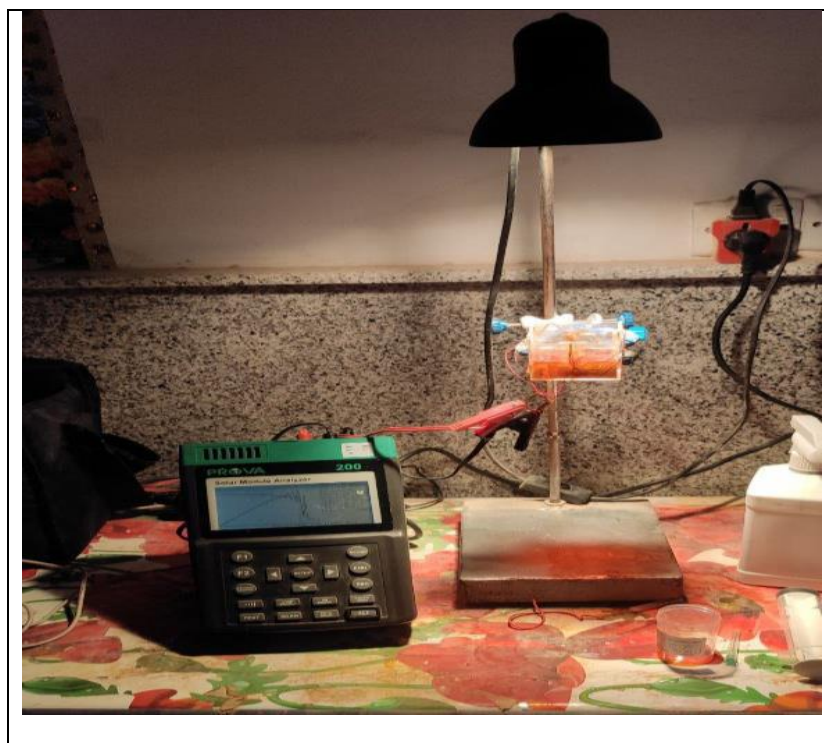


Figure 1.8 energy band gap for  $\gamma\text{-Al}_2\text{O}_3$

#### 4. Results of concentrator on polycrystalline silicon Solar Cells

The silicon solar cell, whose efficiency was to be measured before and after the addition of the nanoparticle concentrator, was prepared by constructing a box with dimensions of 40 mm x 40 mm x 150 mm. Three cells, previously specified, were placed inside it, connected in an antiparallel configuration, and set on an iron stand. Above them, a light source was positioned, and their ends were connected to a Prova 200 efficiency measurement device, as illustrated in Figure 1.9.



**Figure 1.9** show the Silicon cell system

In general, the results of the cell system with the addition of concentrator, recorded a positive change in efficiency, ranging from 16% to 79% for both the  $\gamma$ -aluminum oxide nano ( $\gamma\text{-Al}_2\text{O}_3$  NPs Particle size 27.205 nm through TEM) concentrator, with methyl red dye and the dill (*Anethum graveolens*) plant dye alone, respectively. Table 1.3 indicates details of the change in cell efficiency by adding concentrator, to the cell system. As a result of its readings, the nano aluminum oxide concentrator, recorded a change in efficiency of 62%, while the oxide itself with methyl red dye recorded the highest change of 79.5%, while a change of 27.5% was recorded by adding it with the dye of the dill (*Anethum graveolens*) plant. This increase in efficiency can be attributed to the effective role of nanomaterials. Which works to reduce the waste of solar energy due to its large surface area compared to its bulk counterparts, thus increasing the scattering phenomenon (Raman scattering, for example) and thus directing most of the incident light towards the cell system, while the share of the center of the dill plant alone was the least in the change in efficiency, reaching 15%. While a change of 27.5% was recorded combined with nano aluminum oxide. The reason for the lack of increase in efficiency is attributed to the effect of the relatively large size of the dill plant dye (*Anethum graveolens*) particles, which perhaps led to absorption of a portion of the incident light and reflecting another portion, thus reducing light harvesting towards the silicon cell system (20), (21).

**Table 1.3** showing cell system parameter

Material	Constrictions	V <sub>OPEN</sub> (V)	I <sub>short</sub> (mA )	V <sub>max</sub> (V)	I <sub>max</sub> (mA)	FF	EF%	Δη %	
<b>Empty silicon cell</b>	0.00000 M	0.515	150.0	0.396	136.0	0.345	0.345	0.000	
	0.00151 M	0.549	193.9	0.449	175.8	0.741	0.505	46.377	
	<b>γ-Al<sub>2</sub>O<sub>3</sub></b>	0.00302 M	0.542	201.8	0.448	165.4	0.677	0.474	37.391
		0.00452 M	0.544	195.3	0.448	184.8	0.779	0.53	53.623
		0.00603 M	0.55	219.3	0.458	182.7	0.693	0.536	55.362
		0.00754 M	0.553	205.6	0.445	196	0.767	0.559	62.029
<b>Methyl Red Dye</b>	0.00059 M	0.538	179.4	0.433	153	0.686	0.424	22.899	
	0.00118 M	0.526	171	0.438	163	0.793	0.457	32.464	
	0.00177 M	0.521	144.6	0.471	139.7	0.873	0.421	22.029	
	0.00236 M	0.547	166.4	0.444	154.1	0.751	0.438	26.957	
	0.00295 M	0.549	178.5	0.45	164.2	0.754	0.473	37.101	
<b>Dill (Anethum graveolens) dye</b>	0.0000254 g/ml	0.547	170.3	0.461	143	0.707	0.422	22.319	
	0.0000502 g/ml	0.544	157.5	0.426	153.3	0.762	0.418	21.159	
	0.0000747 g/ml	0.537	174.7	0.44	144.4	0.677	0.407	17.971	
	0.0000989 g/ml	0.53	170.9	0.428	145.8	0.688	0.4	15.942	
	0.0001228 g/ml	0.521	170.3	0.414	150.9	0.704	0.4	15.942	
<b>γ-Al<sub>2</sub>O<sub>3</sub> + Methyl Red Dye</b>	0.001508 M + 0.000571 M	0.544	166.3	0.423	151.8	0.709	0.411	19.100	
	0.003016 M + 0.001142 M	0.543	164.6	0.429	163.5	0.784	0.449	30.100	
	0.004524 M + 0.001713 M	0.549	190.8	0.446	175.5	0.747	0.501	45.200	
	0.006032 M + 0.002284 M	0.557	220.8	0.451	189.8	0.696	0.548	58.800	
	0.007540 M + 0.002855	0.557	227.9	0.449	215.7	0.762	0.62	79.700	
	0.00151 M + 0.0000254 g/ml	0.549	160.8	0.436	157.5	0.777	0.44	27.	
<b>γ-Al<sub>2</sub>O<sub>3</sub> + Dill (Anethum graveolens) dye</b>	0.00302 M + 0.0000502 g/ml	0.547	180.5	0.433	157.6	0.691	0.437	26.700	
	0.00452 M +	0.544	158.2	0.44	155	0.792	0.437	26.700	

Material	Constrictions	V <sub>OPEN</sub> (V)	I <sub>short</sub> (mA )	V <sub>max</sub> (V)	I <sub>max</sub> (mA)	FF	EF%	Δη %
	0.0000747 g/ml							
	0.00603 M + 0.0000989 g/ml	0.542	181.4	0.447	148.7	0.676	0.426	23.500
	0.00754 M + 0.0001228 g/ml	0.545	167.2	0.434	149.3	0.711	0.415	20.300

## 5. Conclusion

Using an electrochemical method, nano-aluminum oxide ( $\gamma$ -Al<sub>2</sub>O<sub>3</sub> NPs) was synthesized and characterized by TEM, FESEM, AFM, UV-Vis, and EDX techniques. When integrated into solar cells as a concentrator, this nano oxide especially when combined with methyl red dye or dill (*Anethum graveolens*) plant dye, significantly boosted efficiency, with the highest increases being 79.7% for ( $\gamma$ -Al<sub>2</sub>O<sub>3</sub>/methyl red dye) and 62% for ( $\gamma$ -Al<sub>2</sub>O<sub>3</sub>) alone. These enhancements are key to advancing solar cell technology and optimizing energy utilization.

## REFERENCES

- [1] 1. Rajput A, Shevalkar G, Pardeshi K, Pingale P. Computational nanoscience and technology. *OpenNano*. 2023;12:100147.
- [2] 2. Kumar A, Jayeoye TJ, Mohite P, Singh S, Rajput T, Munde S, et al. Sustainable and consumer-centric nanotechnology-based materials: An update on the multifaceted applications, risks and tremendous opportunities. *Nano-Structures & Nano-Objects*. 2024;38:101148.

- [3] 3. Noah NM, Ndagili PM. Green synthesis of nanomaterials from sustainable materials for biosensors and drug delivery. *Sensors International*. 2022;3:100166.
- [4] 4. Bhati N, Nazeeruddin MK, Maréchal F. Environmental impacts as the key objectives for perovskite solar cells optimization. *Energy*. 2024;299:131492.
- [5] 5. Oni AM, Mohsin ASM, Rahman MM, Hossain Bhuian MB. A comprehensive evaluation of solar cell technologies, associated loss mechanisms, and efficiency enhancement strategies for photovoltaic cells. *Energy Reports*. 2024;11:3345-66.
- [6] 6. Filatova EO, Konashuk AS. Interpretation of the changing the band gap of Al<sub>2</sub>O<sub>3</sub> depending on its crystalline form: connection with different local symmetries. *The Journal of Physical Chemistry C*. 2015;119(35):20755-61.
- [7] 7. Anggraeni S, Kurniawan F, editors. *Synthesis of aluminium nanoparticles using electrochemical method*. Journal of Physics: Conference Series; 2020: IOP Publishing.
- [8] 8. Khalid M, Shanks K, Ghosh A, Tahir A, Sundaram S, Mallick TK. Temperature regulation of concentrating photovoltaic window using argon gas and polymer dispersed liquid crystal films. *Renewable Energy*. 2021;164:96-108.
- [9] 9. Ejaz A, Babar H, Ali HM, Jamil F, Janjua MM, Fattah IR, et al. Concentrated photovoltaics as light harvesters: Outlook, recent progress, and challenges. *Sustainable Energy Technologies and Assessments*. 2021;46:101199.
- [10] 10. Bouhamed H, Baklouti S. Synthesis and characterization of Al<sub>2</sub>O<sub>3</sub>/Zno nanocomposite by pressureless sintering. *Powder technology*. 2014;264:278-90.
- [11] 11. Al-Byati MKAA, Al-Duhaidahawi AMJ. Synthesis and Characterization of Zinc Oxide Nanoparticles by Electrochemical Method for Environmentally Friendly Dye-Sensitized Solar Cell Applications (DSSCs). *Biomedicine and Chemical Sciences*. 2023;2(1):53-7.
- [12] 12. Arunarajeswari P, Mathavan T, Divya A, Benial AMF. Influence of N-Methylaniline on physicochemical and optical properties of  $\gamma$ -Al<sub>2</sub>O<sub>3</sub> nanoparticles. *Materials Research Express*. 2020;6(12):1250c9.
- [13] 13. Vashista M, Paul S. Correlation between full width at half maximum (FWHM) of XRD peak with residual stress on ground surfaces. *Philosophical Magazine*. 2012;92(33):4194-204.

- [14] 14. Alamouti AF, Nadafan M, Dehghani Z, Ara MHM, Noghreiyani AV. Structural and Optical Coefficients Investigation of  $\gamma$ -Al<sub>2</sub>O<sub>3</sub> Nanoparticles using Kramers-Kronig Relations and Z-scan Technique. *Journal of Asian Ceramic Societies*. 2021;9(1):366-73.
- [15] 15. Zhu D, Wang X, Jia P, Cai C, Huang J, Zhou G. One-dimensional  $\gamma$ -Al<sub>2</sub>O<sub>3</sub> growth from the oxidation of NiAl. *Corrosion Science*. 2023;216:111069.
- [16] 16. Prins R. On the structure of  $\gamma$ -Al<sub>2</sub>O<sub>3</sub>. *Journal of Catalysis*. 2020;392:336-46.
- [17] 17. Scimeca M, Bischetti S, Lamsira HK, Bonfiglio R, Bonanno E. Energy Dispersive X-ray (EDX) microanalysis: A powerful tool in biomedical research and diagnosis. *European journal of histochemistry: EJH*. 2018;62(1).
- [18] 18. Abu-Ghazala AH, Abdelhady HH, Mazhar AA, El-Deab MS. Exceptional room temperature catalytic transesterification of waste cooking oil to biodiesel using environmentally-benign K<sub>2</sub>CO<sub>3</sub>/ $\gamma$ -Al<sub>2</sub>O<sub>3</sub> nano-catalyst. *Chemical Engineering Journal*. 2023;474:145784.
- [19] 19. Klein J, Kampermann L, Mockenhaupt B, Behrens M, Strunk J, Bacher G. Limitations of the Tauc plot method. *Advanced Functional Materials*. 2023;33(47):2304523.
- [20] 20. Pilot R, Signorini R, Durante C, Orian L, Bhamidipati M, Fabris L. A review on surface-enhanced Raman scattering. *Biosensors*. 2019;9(2):57.
- [21] 21. Jain P, Shokeen P, Arun P. Improved efficiency of plasmonic tin sulfide solar cells. *Journal of Materials Science: Materials in Electronics*. 2016;27:5107-13.